Mem. Fac. Eng., Kyoto Univ. Vol. 53, No. 3 (1991)

Analysis of Arc Phenomena in Boundary Layer Of MHD Generator Channel

By

Isao INOUE*, MOTOO ISHIKAWA** and Juro UMOTO**

(Received March 4, 1991)

Abstract

By means of a time-dependent two-dimensional numerical simulation utilizing the Finite Element Method, we study arc phenomena analytically in the boundary layer of the Faraday MHD power generator using petroleum-fired gas plasma as the working fluid, and get the following several results. On the anode side, the calculated values of the electrode voltage drop agree very well with the experimental ones, which demonstrates that the calculation simulates the experiment considerably well. On low temperature electrode, the current flow becomes the big arc with high temperature and large current density. The generation, movement, keeping and disappearance of the arc depend on a balance among the effect of convection, the Hall effect and the braking force based on the Lorentz force. The positions of the generated arc and the behavior of the arc-cycle are decided mainly by the effect of convection and by the electrode temperature. The period of the arc-cycle and the width of the arc are closely connected with the temperature of the electrode wall and the load resistance.

1. Introduction

A Faraday MHD power generator has many segmented electrodes to prevent short-circuit of the Hall electric field. Since the electrodes are usually cooled by using water, there is generated thermal boundary layer near their surfaces in the working gas flowing in the channel. The electrical conductivity of the gas near the electrode depends strongly on its temperature, which is very low compared to that of the core flow. The corrent flow is locally concentrated while it passes through a low conductible region in the boundary. Since an arc spot appears in the current concentration, the impedance in it is decreased. The arc spots appear on the anode and the cathode. Also on the high temperature cathode, there is the possibility that an arc spot will be generated to provide local thermionic emission from it. On the other hand, on the anode no spot is generated, because many electrons go into the working gas plasma in the channel and it is thought that the current flows into the

* Yatsushiro National College of Technology.
** Department of Electrical Engineering.

high temperature anode in the diffusing mode. From the above, it can be seen that states of the arcs depend on temperature, material and etc. of the electrodes.

About the arc discharge in the boundary layer in the MHD generator, there have been many experimental and theoretical investigations[1)~7)]. A large number of experimental results were investigated from the view point of the arc characteristics; one analytical method[8)] for the arc was proposed, and a study[9)] of arc characteristics was done by dividing the boundary layer into three regions. Several papers[10),11)] reported numerical simulation of performance of the arc moving on the electrode in the boundary layer. It has been experimentally found, however, that the behavior of the arc is a very complicated phenomenon, and there are still many aspects which must be theoretically clarified. Also, the numerical simulation of the behavior of the arc near the electrode is appropriate for making its characteristics clear.

The purpose of the present paer is to carry out a two-dimensional time-dependent numerical simulation[12),13)] of arc phenomena occuring in the boundary of the Faraday MHD generator[14)] of practical size using a petroleum-fired gas. By this simulation, we theoretically analyse the mechanism of the current flow and the performance characteristics of the arc discharge near the electrode wall for various wall temperatures and compare the theoretical results with the experimental ones.

2. Theoretical Model

2.1 Basic equations

The basic equations for the working gas in the generator channel are the Maxwell's equations and the generalized Ohm's law, namely

$$\text{rot } \boldsymbol{E} = 0 \tag{1}$$

$$\text{div } \boldsymbol{J} = 0 \tag{2}$$

$$\boldsymbol{J} = \sigma(\boldsymbol{E} + \boldsymbol{u} \times \boldsymbol{B}) - (\beta/B)(\boldsymbol{J} \times \boldsymbol{B}) \tag{3}$$

where $\boldsymbol{J}$ is the current density, $\boldsymbol{E}$ the electric field, $\boldsymbol{u}$ the gas velocity, $\boldsymbol{B}$ the applied magnetic flux density, and σ and β are the electrical conductivity and the Hall parameter, repectively

The gas temperature is governed by the following equation of energy conservation

$$\begin{aligned} \rho C_p \left(\frac{\partial T}{\partial t} + \boldsymbol{u} \cdot \nabla T \right) &= \kappa_e \nabla^2 T + \boldsymbol{J} \cdot \boldsymbol{E} \\ &= \kappa_e \nabla^2 T + \frac{\boldsymbol{J}^2}{\sigma} + \boldsymbol{u} \cdot (\boldsymbol{J} \times \boldsymbol{B}) \end{aligned} \tag{4}$$

where ρ is the total mass density, C_p the specific heat at constant pressure, T the gas temperature, κ_e the effective thermal conductivity.

2.2 Assumptions

Figure 1 shows one electrode-pitch of a Faraday MHD generator with the x, y and z coordinate axes used in the calculations.

Here, to simplify the basic equations and carry out a two-dimensional numerical analysis, the following assumptions are introduced.

(1) All physical quantities satisfy the periodicity in the flow direction (x direction) per one electrode-pitch and also their values are constant in the direction of the magnetic field (z direction).

(2) The anode and the cathode have the same physical characteristics.

(3) The magnetic flux density $\boldsymbol{B}$ is constant in space and time, and its form is

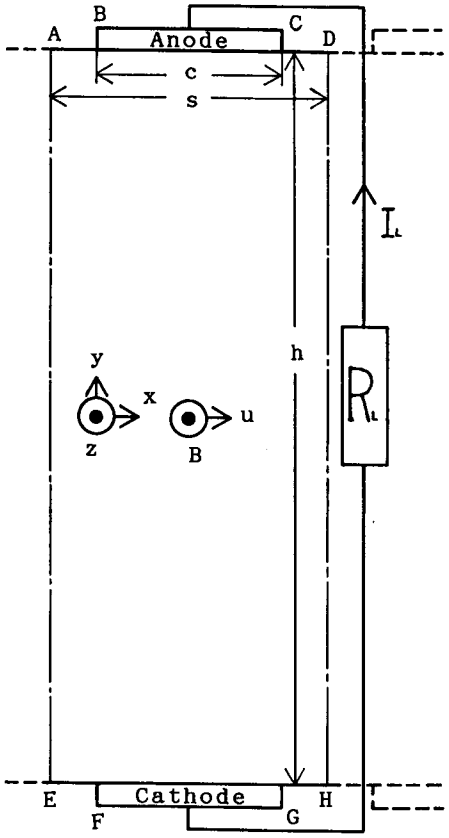

Fig. 1. One electrode-pitch of Faraday MHD generator and coordinate system.

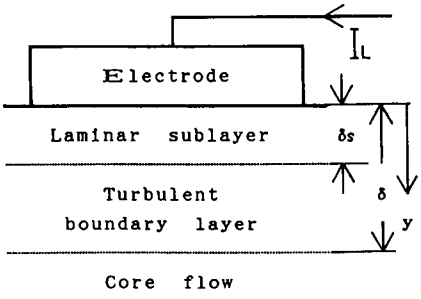

Fig. 2. Arrangement near electrode.

$$\boldsymbol{B} = (0, 0, B), \qquad B = |\boldsymbol{B}| \tag{5}$$

(4) The laminar sublayer region exists on the electrode walls in the boundary layer as shown in Fig. 2.

(5) The gas velocity $\boldsymbol{u}$ is constant in time, and its form is

$$\boldsymbol{u} = (u, 0, 0), \qquad u = |\boldsymbol{u}| \tag{6}$$

Also, the distribution of the initial gas velocity is as follows:

$$u = \left\{ \begin{array}{ll} u_\infty = \text{constant} & \text{(in the core flow)} \\ u_\infty (y/\delta)^{1/7} & \text{(in the turbulent boundary layer)} \\ u_\infty (y/\delta_s)(\delta_s/\delta)^{1/7} & \text{(in the laminar sublayer region)} \end{array} \right\} \tag{7}$$

where y is the distance from the electrode wall, δ and δ_s are the thicknesses of the boundary layer and the laminar sublayer, respectively.

(6) The initial gas temperature T is as follows:

$$T = \left\{ \begin{array}{ll} T_\infty = \text{constant} & \text{(in the core flow)} \\ T_w + (T_\infty - T_w)(y/\delta)^{1/7} & \text{(in the turbulent boundary layer)} \\ T_w + (T_\infty - T_w)(y/\delta_s)(\delta_s/\delta)^{1/7} & \text{(in the laminar sublayer region)} \end{array} \right\} \tag{8}$$

where T_w is the temperature of the electrode wall.

(7) The effective thermal conductivity κ_e is as follows:

$$\kappa_e = \left\{ \begin{array}{ll} \kappa_\infty = \text{constant} & \text{(in the core flow)} \\ (\kappa \rho l^2/\mu)(\partial u/\partial y) & \text{(in the turbulent boundary layer)} \\ \kappa & \text{(in the laminar sublayer region)} \end{array} \right\} \tag{9}$$

where the thermal conductivity κ, the viscosity μ and the mixing length l are given by the following equations

$$\left. \begin{array}{l} \kappa = -0.7689 + 0.05307\, T^{1/2} - 1.123 \times 10^{-3} T + 8.661 \times 10^{-6} T^{3/2} \\ \mu = 1.939 \times 10^{-5} + 2.110 \times 10^{-6} T^{1/2} - 1.303 \times 10^{-8} T + 1.537 \times 10 T^{3/2} \\ l = 0.125 (y_1 - y_2) \end{array} \right\} \tag{10}$$

where

$$\left. \begin{array}{l} y_1 = y \quad \text{when} \quad (u - u_L)/(u_u - u_L) = 0.9 \\ y_2 = y \quad \text{when} \quad (u - u_L)/(u_u - u_L) = 0.1 \end{array} \right\} \tag{11}$$

and where u_L and u_u are the lower and the upper velocities in the laminar flow, respectively.

(8) The electrical conductivity σ and the Hall parameter β of the working gas are given by the following equations

$$\left.\begin{aligned}\sigma &= 89.9\,p^{-0.51}\,T^{1.005}\exp(-2.52\times10^4/T)\\ \beta &= 4.43\,B\,p^{-0.99}\,T^{0.97}\end{aligned}\right\} \tag{12}$$

where p is the static pressure.

2.3 Current stream function

In analyzing phenomena near the wall, the current stream function $\Psi = \Psi(x, y)$ defined by the following equations is used to decrease the number of the unknown variables.

$$\left.\begin{aligned}J_x &= -(I_L/W)(\partial\Psi/\partial x)\\ J_y &= (I_L/W)(\partial\Psi/\partial y)\end{aligned}\right\} \tag{13}$$

where I_L is the load current and W the channel width. Using the above assumptions, Eq. (3) is reduced to the following set

$$\left.\begin{aligned}E_x &= (J_x - \beta J_y)/\sigma\\ E_y &= (-\beta J_y + J_y)/\sigma + uB\end{aligned}\right\} \tag{14}$$

By substituting Eqs. (13) and (14) into Eq. (2), we get

$$\frac{1}{\sigma}\left\{\frac{\partial}{\partial x}\left(\frac{\partial\Psi}{\partial x}+\beta\frac{\partial\Psi}{\partial y}\right)-\frac{\partial}{\partial y}\left(\beta\frac{\partial\Psi}{\partial x}-\frac{\partial\Psi}{\partial y}\right)\right\}=0 \tag{15}$$

To solve Eq. (15), the boundary conditions have to be given along the perimeter of the calculation domain □ AHED, which is show in Fig. 1. The boundary condition on the electrode surfacs $\overline{BC}$ and $\overline{FG}$ is $E_x = 0$, and so it is transformed by Eqs. (13) and (14) as follows:

$$\beta(\partial\Psi/\partial x) - (\partial\Psi/\partial y) = 0 \quad (\text{on } \overline{AB} \text{ and } \overline{EF}) \tag{16}$$

Since $J_y = 0$ on the insulator surfaces $\overline{AB}$, $\overline{CD}$, $\overline{EF}$ and $\overline{GH}$, $\Psi =$ constant on them is obtained by using Eq. (13). Then, the value of Ψ is taken as equal to zero on the $\overline{AB}$ and $\overline{EF}$, namely

$$\Psi = 0 \quad (\text{on } \overline{AB} \text{ and } \overline{EF}) \tag{17}$$

The integration of J_y along $\overline{BC}$ or $\overline{FG}$ gives the load current I_L, and so using Eq. (13), we get

$$I_L = -W\int_B^C J_y\,dx = W\int_B^C \frac{I_L}{W}\frac{\partial\Psi}{\partial x}\,dx = I_L\{\Psi(C) - \Psi(B)\} \tag{18}$$

By Eqs.(17) and (18), we acquire

$$\Psi = 1 \quad (\text{on } \overline{CD} \text{ and } \overline{GH}) \tag{19}$$

Since the periodicity per one electrode-pitch is assumed, the boundary conditions on $\overline{DH}$ and $\overline{AE}$ satisfy the following relation

$$\Psi(\text{on } \overline{DH}) - \Psi(\text{on } \overline{AE}) = 1 \tag{20}$$

Considering that each anode-cathode pair is connected to the external load R_L as shown in Fig. 1, the load current I_L is obtained as follows:

$$I_L = \int_0^h uBdy \Big/ \left\{ R_L + \frac{1}{W}\int_0^h \frac{1}{\sigma}\left(\frac{\partial \Psi}{\partial x} + \beta\frac{\partial \Psi}{\partial y}\right)\Big|_{x=s/2} dy \right\} \tag{21}$$

by using Eq.s (13) and (14), where h is the channel height and s the one electrode-pitch length.

2.4 Gas temperature conditions

By the assumptions given in Section 2.2, Eq.(4) is reduced as follows:

$$\rho C_p\left(\frac{\partial T}{\partial t} + u\frac{\partial T}{\partial x}\right) = \kappa_e\left(\frac{\partial^2 T}{\partial x^2} + \frac{\partial^2 T}{\partial y^2}\right) + \frac{J_x^2 + J_y^2}{\sigma} + uBJ_y \tag{22}$$

The boundary conditions for the gas temperature T are given as follows:

$$\begin{aligned} &T = T_w = \text{constant} \quad (\text{on } \overline{AD} \text{ and } \overline{EH}) \\ &T(\text{on } \overline{AE}) = T(\text{on } \overline{DH}) \end{aligned} \tag{23}$$

2.5 Numerical analysis

In this analysis, we solve Eqs.(15) and (22) by the Finite Element Method. The

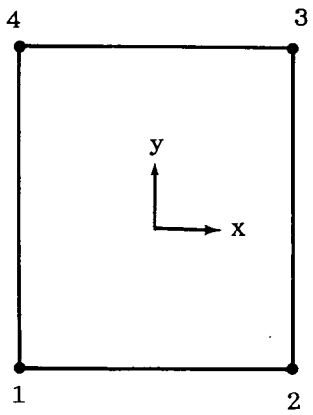

Fig. 3. Rectangular element.

analytical region S is divided into subregions which consist of the rectangular bilinear elements S^e's as shown in Fig. 3. In each element, the stream function $\Psi = \Psi(x, y)$ is expressed by its values Ψ_1 to Ψ_4 at the four nodes 1 to 4, respectively, in S^e and interpolation function $N_1 = N_1(x, y)$ to N_4 (x, y) decided by the coordinates of the above nodes 1 to 4, respectively, as follows:

$$\Psi(x, y) = \{N(x, y)^\top\}\{\Psi^e\} \tag{24}$$

where

$$\left.\begin{aligned} &\{N(x, y)\}^\top = \{N_1(x, y), \cdots, N_4(x, y)\} \\ &\{\Psi^2\} = \{\Psi_1, \Psi_2, \Psi_3, \Psi_4\}^\top \end{aligned}\right\} \tag{25}$$

In this analysis, the Galerkin process is used because Eq. (15) does not have the functional. So it is assumed that for a node i contained in the analytical region S, the weighted integral of Eq. (15) with the weight $N_i(x, y)$ over S, which is the summation of the interpolation functions corresponding to the node i, becomes 0. Therefore, the followng equation is obtained.

$$\iint_S \frac{N_i}{\sigma}\left\{\frac{\partial}{\partial x}\left(\frac{\partial \Psi}{\partial x} + \beta\frac{\partial \Psi}{\partial y}\right) - \frac{\partial}{\partial y}\left(\beta\frac{\partial \Psi}{\partial x} - \frac{\partial \Psi}{\partial y}\right)\right\} dxdy = 0 \tag{26}$$

By applying the Gauss' divergence theorem to the result partially integrating Eq. (26), we get

$$\begin{aligned} &\iint_S \frac{1}{\sigma}\left\{\frac{\partial N_i}{\partial x}\left(\frac{\partial \Psi}{\partial x} + \beta\frac{\partial \Psi}{\partial y}\right) - \frac{\partial N_i}{\partial y}\left(\beta\frac{\partial \Psi}{\partial x} - \frac{\partial \Psi}{\partial y}\right)\right\} dxdy \\ &\qquad + \oint_C (N_i E_x dx + N_i E_y dy) = 0 \end{aligned} \tag{27}$$

where C is the contour of the region S.

Dividing the region S and its contour C into a number of elements and substituting Eq. (24) into Eq. (27), the following equation is obtained.

$$\Sigma([K^e]\{\Psi^e\} + \{F^e\}) = 0 \tag{28}$$

where

$$\left.\begin{aligned} [K^e] &= \iint_{S^e} \frac{1}{\sigma}[\{N_x\}(\{N_x\}^\top + \beta\{N_y\}^\top) - \{N_y\}(\beta\{N_x\}^\top - \{N_y\}^\top)]\, dxdy \\ \{F^e\} &= \oint_{C^e} (\{N\} E_x dx + \{N\} E_y dy) \\ \{N_x\} &= \partial\{N\}/\partial x, \qquad \{N_y\} = \partial\{N\}/\partial y \end{aligned}\right\} \tag{29}$$

in which C^e is the contour of the element S^e.

Solving the simultaneous equations given by Eq.(28) under some given conditions, the values of Ψ at every node are obtained.

Next, the same procedure can be used to calculate the gas temperature. Accordingly the temperature $T = T(x, y)$ in S^e is given by

$$\left.\begin{aligned} T(x, y) &= \{N(x, y)\}^{\top}\{T^e\} \\ \{T^e\} &= \{T_1, T_2, T_3, T_4\}^{\top} \end{aligned}\right\} \tag{30}$$

where T_1 to T_4 are the temperatures of the four nodes 1 to 4, respectively, in S^e.

By applying the Galerkin process and the Gauss' divergence theorem to Eq.(22) and using Eq.(30), Eq.(22) is transformed as follows:

$$\Sigma([G^e]d\{T^e\}/dt + [K^e]\{T^e\} - \{F^e\}) = 0 \tag{31}$$

where

$$\left.\begin{aligned} [G^e] &= \iint_{S^e} \rho C_p \{N\}\{N\}^{\top} dxdy \\ [K^e] &= \iint_{S^e} \kappa_e(\{N_x\}\{N_x\}^{\top} + \{N_y\}\{N_y\}^{\top} + \rho C_p u\{N\}\{N_x\}^{\top})dxdy \\ \{F^e\} &= \iint_{S^e} \frac{J^2}{\sigma}\{N\}\,dxdy + \oint_{C^e} D_n\{N\}\,ds \end{aligned}\right\} \tag{32}$$

in which D_n is the quantity of heat to transfer from an element.

Eq.(31) is rewritten as follows:

$$[G]d\{T\}/dt + [K]\{T\} = \{F\} \tag{33}$$

By applying the Crank-Nicolson method to te above equation, it is transformed into the following form

$$([G]/\Delta t + [K]/2)\{T(t + \Delta t)\} = ([G]/\Delta t - [K]/2)\{T(t)\} + \{F\} \tag{34}$$

3. Results and Discusions

3.1 Geometrical and gasdynamic Conditions

In order to compare numerical results with experimental ones, the dimensions of the channel used in the numerical calculation are chosen equal to those of the ETL-Mark VII B-channel: the channel height $h = 240$ mm, the channel width $W = 75$ mm, one electrode-pitch $s = 24$ mm and the electrode width $c = 20$ mm. Also, the gasdynamic conditions are chosen to have almost the same values as the experimental ones: the applied magnetic flux density $B = 2.5$ T, the gas core flow

temperature T_∞ = 2,500 K, the same velocity u_∞ = 800 m, the static pressure p = 1 atm, boundary layer thickness δ = 30 mm, laminar sublayer thickness δ_s = 1.0 mm and the thermal conductivity κ_∞ = 1.2 W/m·K. In this connection, one electrode-pitch region in Fig. 3 is divided into 24 × 46 or 24 × 50 mesh uniformly and nonuniformly in x and y directions, respectively. The time step Δt is selected 10 μs to satisfy the stability condition.

3.2 Behaviors and characteristics of arc

In experiments, the current density is about 1.5 A/cm^2 in the channel of the MHD generator and the arcs are generated as points on the anode. Similar phenomena are shown by numerical calculation, where for time $t < 0$ the current density is set to about 1.5 A/cm^2 and an arc spot is assumed to be produced on the anode, and for $t > 0$ the electrical and fluid quantities in the channel are calculated.

Figures 4 and 5 show the time-dependent variations of the distributions of the current and the temperature T, respectively, in the boundary layer for the wall temperature T_w = 500 K and the load resistance R_L = 5 Ω. As seen in Fig. 4., an arc appears just at the upstream edge anode, then moves to the downstream edge of the electrode and disappears soon after. At the same time, a new arc generates at the upstream edge, and repeats the same process. The behavior of the arc on a cathode is similar to the arc on the anode. The periods of one arc-cycle (generate-move-disappear-generate) on the anode and the cathode, respectively, are about 470 and

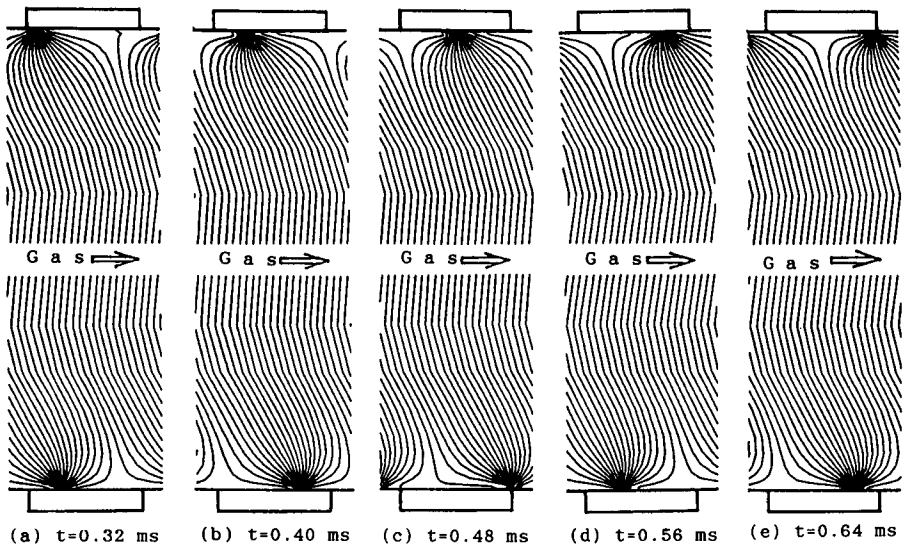

Fig. 4. Time-dependent current distributions in boundary layer for T_w = 500 K, R_L = 5Ω and $\Delta\Psi$ = 1.13A.

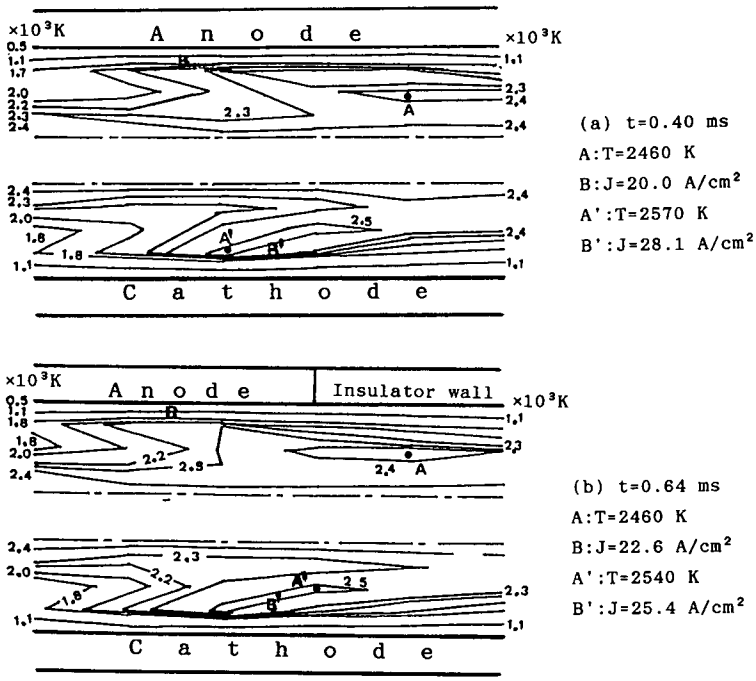

Fig. 5. Time-dependent temperature distributions in laminar sublayer for $T_w = 800$ K and $R_L = 5\ \Omega$.

230 μs, where the periods include the holding time of about 40 μs at the downstream edge. The period on the anode is considerably long compared to the one on the cathode.

The above phenomena depend on a balance got between the effect of convection, the Hall effect and the braking force based on the Lorentz force. Our calculated results simulate considerably well the experimental results. However, since the three-dimensional effect in the experiment and the interaction between the gas flow and electrical quantities are neglected in the calculation, the period of one arc-cycle becomes relatively short compared with the real one.

In our calculation, the electrode voltage drop on the anode is about 95 V at the current density $J_y = -1.24$ A/cm^2. The experimental value is about 80 V at the same current density, and so the calculated result is a little higher than the experimental one.

From Fig. 5. and the other calculated results, it is seen that the temperatures of the arcs on the anode and the cathode sides become about 2240 to 2460 and 2350 to 2570 K, respectively, and the current density of the arcs on the anode and the cathode sides become about 17.1 to 23.1 and 25.4 to 30.0 A/cm^2, respectively. This

shows that the arcs generated in the boundary layer grow into big arcs of high temperature and large current density under the condition of a wall temperatue of 500 K.

Figures 6 and 7 show a time-dependent variation of the distributions of the current and the temperature T, respectively, in the boundary layer for $T_w = 800$ K and $R_L = 2\ \Omega$. As seen in Fig. 6., on the anode side, the arc appears on its upstream side, and then moves downstream. The arc is generated and kept at about two thirds of the electrode width c. At this time, two arcs are recognized in the boundary layer. Namely it is seen that the first old arc is held on the anode while moving downstream and at the same time another new one is being generated on the upstream side of the anode. Since the former transfers its energy to the latter, it becomes smaller and smaller and eventually disapears. The new arc moves downstream and is kept on the electrode, then it shifts again to the upstream side, and is kept there. Next, it moves to te downstream side and there it is kept, and them the same process repeats. Finally, the arc is fixed with a width of 2 to 3 mm on the anode at about a third of the width from the upstream edge.

On the other hand, on the cathode side, an arc appears just at its upstream edge, then moves to the downstream edge and disappears after it is kept for about 100 μs. At the same time a new arc generates at the upstream edge, then shifts and disappears, and again the same process repeats. The period of one arc-cycle is

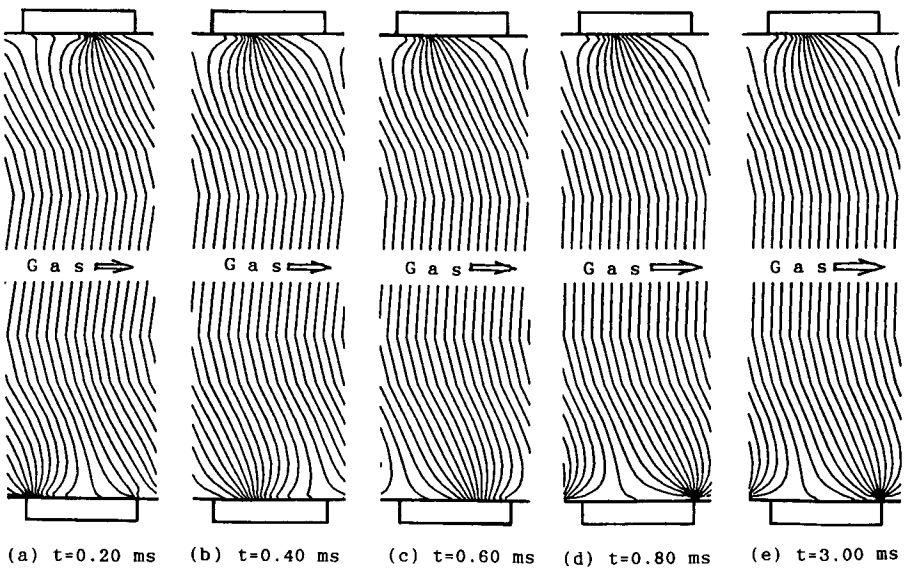

Fig. 6. Time-dependent current distributions in boundary layer for $T_w = 800$ K, $R_L = 2\ \Omega$ and $\Delta\Psi = 2.15$ A.

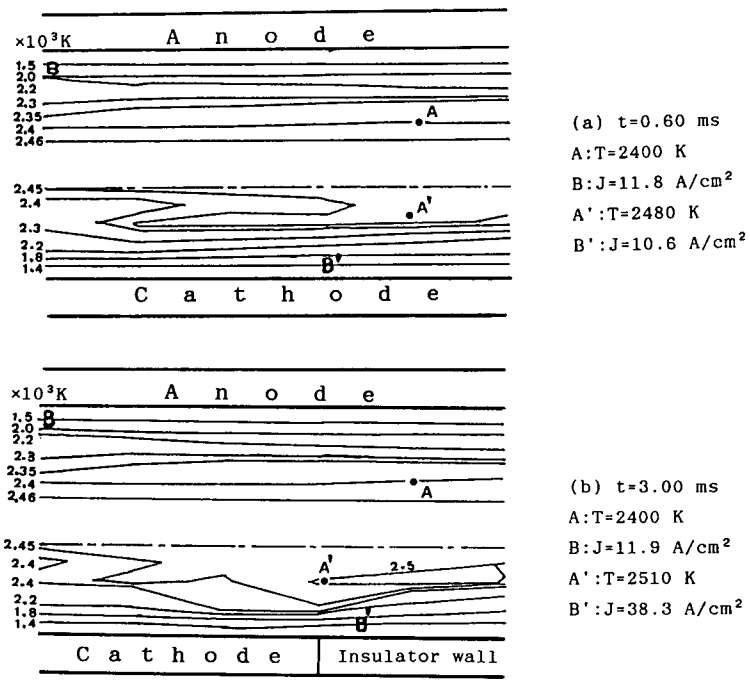

Fig. 7. Time-dependent temperature distributions in laminar sublayer for $T_w = 800$ K and $R_L = 2\ \Omega$.

about 160 μs.

The calculated voltage drop on te anode is about 88 V, and the experimental value about 86 V. This shows that the calculated result agrees very well with the experimental one.

From Fig. 7. and the other many calculated results, it is known that the temperatures of the arcs on the anode and the cathode are about 2400 to 2560 and 2480 to 2650 K, respectively. The current densities in the arcs on the anode and the cathode are about 11.0 to 14.9 and 11.4 to 40.2 A/cm^2, respectively.

The above-mentioned numerical simulation represents the occurrence of the big arc discharge fixed on the anode with a width of 2 to 3 mm at $T_w = 800$ K. The reason why the big arc is fixed on the anode is explained as follows. While the arc is moving downstream on the anode, the effect of convection is decreased gradually by the influences of the wall temperature and the thermal conduction, and so the arc is kept on the downstream side by an equilibrium given between the effect of convection, the Hall effect and the Lorentz force. Since the effect of convection is more decreased by the same reason as the above, the arc is shifted to the upstream side of the anode by the stronger action of the Hall effect. Then, because the

temperature gradient in the arc becomes gradually larger during the movement of the arc to the upstream side, the arc stops on the upstream side due to the aforementioned equilibrium. Then, the arc moves downstream to have a large temperature gradient on the anode by the effect of convection, and then the same process repeats. Finally, the arc is kept with a width of 2 to 3 mm on the anode by the balance between the effect of convection, the Hall effect and the Lorentz force.

Next, Figures 8 and 9 show the time-dependent variation of the distributions of the current and the temperature T, respectively, in the boundary layer for the T_w = 1200 K and $R_L = 2\ \Omega$. As shown in the figures, an arc appears on the anode on its up-stream side and then moves downstream along the gas flow, and is kept in about the center of the anode without arriving at the downstream edge. At this time, there are recognized two arcs on the anode. Namely the one is kept in he central part to have some decreased current density, and the other is generated newly on the upstream side. Since the former transfers its energy to the latter, it becomes smaller and smaller and eventually disappears. The new arc is generated at about a third of the electrode width from the upstream edge, where is is kept for about 80 μs. During this time, its a temperature and current density increase, and it grows into a big arc with high temperature and large current density. Then it shifts to the downstream side, is kept there and disappears in the central part of the electrode, and then the same process repeats. In this connection, the period of one arc-cycle is about 420 μs.

On the other hand, on the cathode, only one arc generates on the upstream side, and then moves downstream and is kept at the downstream edge. After one process, the arc is kept steady at the above edge with high temperature and large current density. Also, the calculated voltage drop on the anode is about 70 V, which agrees very well with the experimental value of about 75 V. This shows that there is a close relation between the experimental and the calculated results.

From Fig. 9. and the other many calculated results, it is seen that the temperatures of the arcs on the anode and the cathode are about 2470 to 2630 and 2860 to 2870 K, respectively. The current densities in the arcs on the anode and the cathode are about 14.1 to 32.1 and 40.1 to 41.2 A/cm^2, respectively. This indicates generation of the big arc discharge.

The results obtained by the similar simulation in the case where the load resistance R_L is changed are in good agreement with the above.

Also, because the period of one arc-cycle on the anode 420 μs is a very short time compared to 1 s, it can be considered that the arc has a current concentration with a narrow width of about 2.5 mm on the electrode. Accordingly, our simulation result presents the narrow arc discharge with high temperature and large

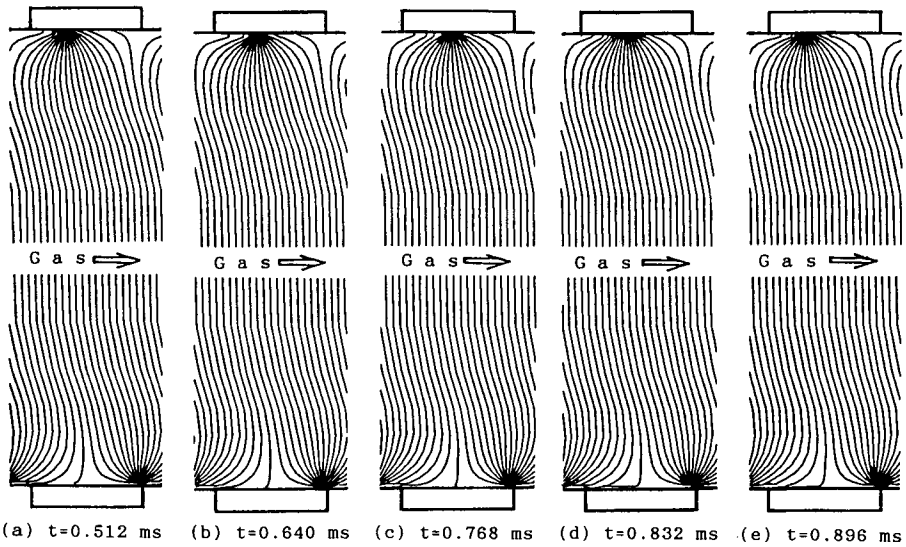

Fig. 8. Time-dependent current distributions in boundary layer for $T_w = 1200$ K, $R_L = 2\ \Omega$ and $\Delta\Psi = 1.59$ A.

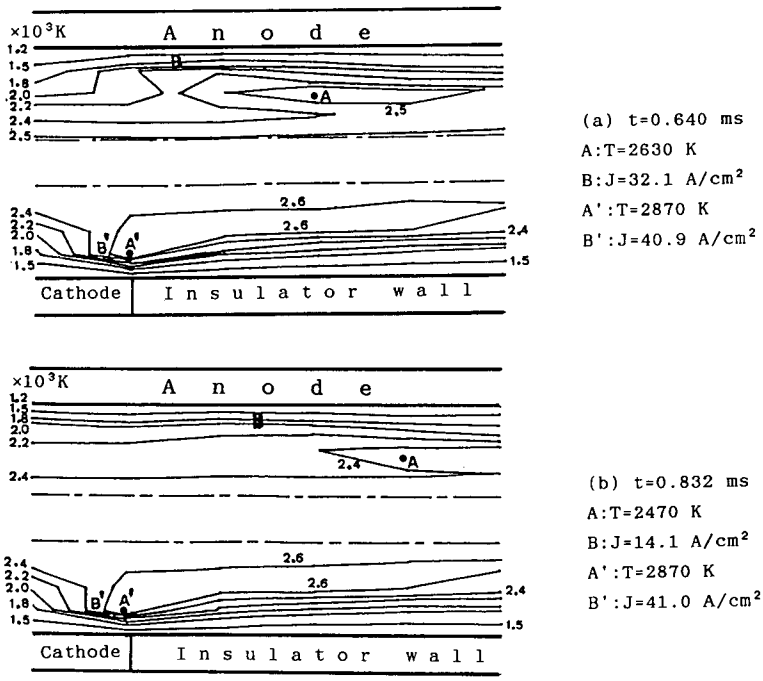

Fig. 9. Time-dependent temperature distributions in laminar sublayer for $T_w =$ 1200 K and $R_L = 2\ \Omega$.

current density.

As previously mentioned, the position of the anode is changed repeatedly from about a third of its width to the central place on the anode. This phenomenon is explained as follows. When the arc kept on the upstream side of the anode has a large temperature gradient, the arc begins to move down-stream on the anode, depending on a balance between the effect of convection, the Hall effect and the Lorentz force. While the arc is moving downstream, the temperature gradient of the arc is gradually relaxed by the influence of the wall temperature and the thermal conduction. Therefore, since the effect of convection is weakened, the arc is kept on the anode by some equilibrium between the one, the Hall effect and the Lorentz force. For the above reason, the temperature gradient of the arc is further relaxed, the Hall effect acts more strongly, the arc on the anode disappears little by little and a new arc occurs on the upstream side of the anode and follows the same process again.

4. Conclusions

The main conclusions, which have been obtained by the above mentioned time-dependent two-dimensional analysis, are as follows:

(1) On the anode side, the calculated values of the electrode voltage drop agree very well with the experimental ones, which demonstrates that the calculation simulates the experiment considerably well.

(2) On the low temperature electrode, the current flow becomes the big arc with a high temperature and a large current density.

(3) Generation, movement, keeping and disappearance of the arc depend on a balance between the effect of convection, the Hall effect, and the braking force based on the Lorentz force.

(4) The positions of the generated arc and the behavior of the arc-cycle are decided mainly by the effect of convection and by the electrode temperature.

(5) The period of the arc-cycle and the width of the arc are closely concerned with the temperature of the electrode wall and the load resistance.

Acknowledgements

The numerical computations were carried out by the super computers in the Data Processing Center, Kyoto University.

References

1) D. A. Oliver; Proc. of 15th Symp. on Eng. Aspects of MHD (1976)
2) R. Hernberg, et al.; 8th Int. Conf. on MHD Electrical Power Generation, 231 (1983)
3) G. Zankl; Proc. of 14th Symp. on Eng. Aspects of MHD, I.1.1 (1974)
4) N. Kayukawa, et al,; 9th Int. Conf. on MHD Electrical Power Generation, **II**, 449 (1986)
5) E. Schmitt, et al.; 10th Int. Conf. on MHD Electrical Power Generation, **I**, V. 34 (1989)
6) B. Gupta, et al.; 10th Int. Conf. on MHD Electrical Power Generation, **I**, V.114 (1989)
7) T. Hara, et al.; 9th Int. Conf. on MHD Electrical Power Generation, **II**, 658 (1986)
8) R. J. Rosa; 9th Int. Conf. on MHD Electrical Power Generation, **II**, 637 (1986)
9) I. Sadovnik, et al.; Proc. of 19th Symp. on Eng. Aspects of MHD, 10.1.1 (1981)
10) M. Ishikawa, et al.; 10th Int. Conf. on MHD Electrical Power Generation, **I**, V.74 (1989)
11) M. Ishikawa, et al.; Proc. of 28th Symp. on Eng. Aspects of MHD, IV. 5–1 (1990)
12) I. Inoue, et al.; Electrical Engineering in Japan, **109**, 119 (1989)
13) I. Inoue, et al.; 10th Int. Conf. on MHD Electrical Power Generation, **I**, V.61 (1989)
14) Y. Kusaka, et al.; 8th Int. Conf. on MHD Electrical Power Generation, **I**, B.1 (1983)